

# Inversion-DPO: Precise and Efficient Post-Training for Diffusion Models

Zejian Li<sup>1</sup> Yize Li<sup>1</sup> Chenye Meng<sup>1</sup> Zhongni Liu<sup>2</sup> YangLing<sup>3</sup>  
 Shengyuan Zhang<sup>1</sup> Guang Yang<sup>4</sup> Changyuan Yang<sup>4</sup>  
 Zhiyuan Yang<sup>4</sup> Lingyun Sun<sup>1</sup>

<sup>1</sup> Zhejiang University <sup>2</sup> University of Electronic Science and Technology of China <sup>3</sup> Peking University <sup>4</sup> Alibaba Group  
 zhejianglee@zju.edu.cn, 1101200212@stu.jiangnan.edu.cn

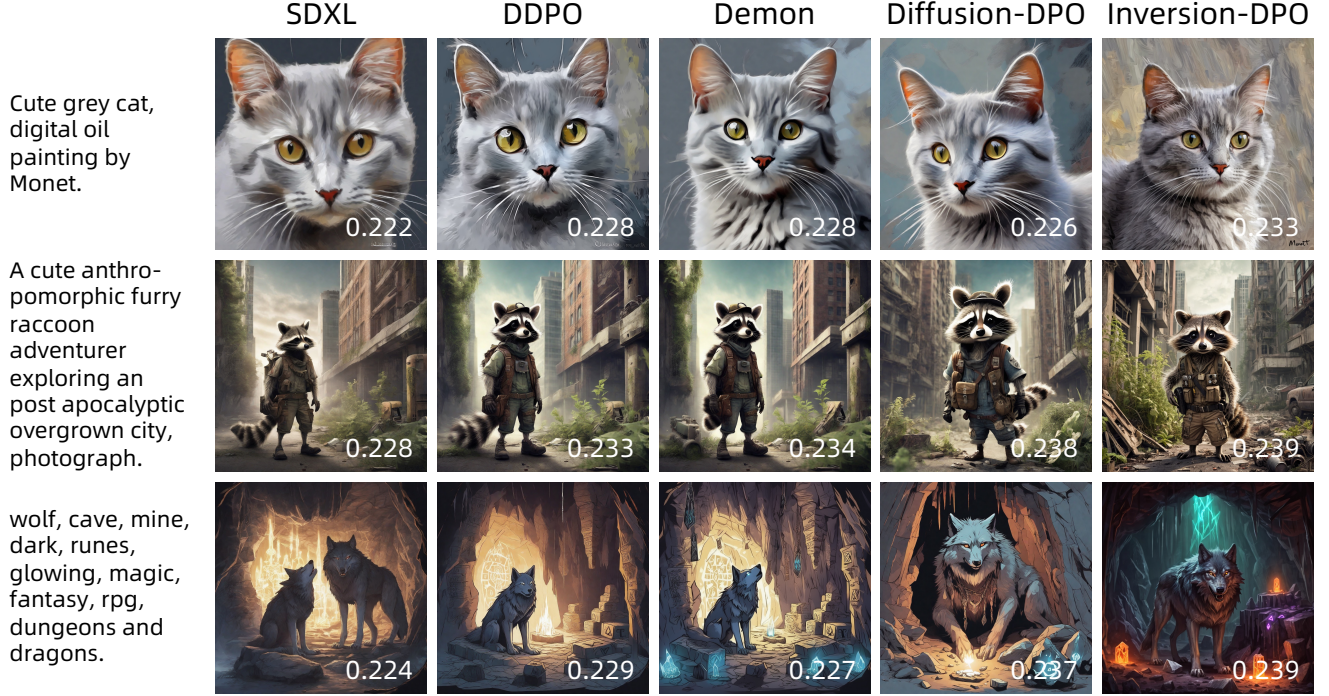


Figure 1. Visual comparison of different baselines and Inversion-DPO. Each image is annotated with PickScore<sup>†</sup> at the bottom right. Inversion-DPO outperforms the baselines in both human visual perception and metric evaluation.

## Abstract

Recent advancements in diffusion models (DMs) have been propelled by alignment methods that post-train models to better conform to human preferences. However, these approaches typically require computation-intensive training of a base model and a reward model, which not only incurs substantial computational overhead but may also compromise model accuracy and training efficiency. To address these limitations, we propose Inversion-DPO, a novel alignment framework that circumvents reward modeling by reformulating Direct Preference Optimization (DPO) with DDIM inversion for DMs. Our method conducts intractable

posterior sampling in Diffusion-DPO with the deterministic inversion from winning and losing samples to noise and thus derive a new post-training paradigm. This paradigm eliminates the need for auxiliary reward models or inaccurate approximation, significantly enhancing both precision and efficiency of training. We apply Inversion-DPO to a basic task of text-to-image generation and a challenging task of compositional image generation. Extensive experiments show substantial performance improvements achieved by Inversion-DPO compared to existing post-training methods and highlight the ability of the trained generative models to generate high-fidelity compositionally coherent images. For the post-training of compositional image ge-

neation, we curate a paired dataset consisting of 11,140 images with complex structural annotations and comprehensive scores, designed to enhance the compositional capabilities of generative models. Inversion-DPO explores a new avenue for efficient, high-precision alignment in diffusion models, advancing their applicability to complex realistic generation tasks. Our code is available at <https://github.com/MIGHTYEZ/Inversion-DPO>

## 1. Introduction

Diffusion models (DMs) [6, 7, 21, 32, 43, 46, 48, 53, 76] have achieved state-of-the-art performance in image generation. This advancement is largely attributed to recent developments in alignment methods of DMs [8, 22, 28, 29, 55, 63, 72], which enable models to be fine-tuned to better align with specific standards or human preferences. These methods typically require training two models simultaneously: a base model and a reward model. While this training paradigm incentivizes superior model performance, it also introduces significant computational overhead.

Diffusion-DPO [57] reparameterizes the reward score into the loss function of the base diffusion model, eliminating the need for an auxiliary model and establishing a new paradigm for DMs to learn from human preferences. However, we identify a post-training issue in Diffusion-DPO, primarily due to its approximation of the reverse process using the forward distribution during derivation. This approximation leads to suboptimal computational accuracy and inefficient training.

To overcome this limitation, we draw insights from DDIM inversion [52] to establish a precise alignment framework for diffusion model fine-tuning. Our Inversion-DPO method fundamentally enhances approximation accuracy by adopting DDIM Inversion to approximate the reverse process  $p_\theta(x_{1:T}|x_0)$ . This proposal eliminates the distributional mismatch inherent in previous approaches, improving approximation accuracy of sampling trajectories reversely from a sample  $x_0$  to inversion samples  $x_{1:T}$ .

Such precision further translates to substantial efficiency gains through simplification of the final loss. By leveraging the trajectory of DDIM Inversion, our method reduces the original four KL divergence terms in Diffusion-DPO’s derivation to two matching terms between aligned model predictions and reference model prediction. This enables more than  $2\times$  faster training convergence compared to baseline implementations. The efficiency improvements are particularly crucial for large-scale diffusion models like SDXL [43], where traditional approximation methods incur high computational costs.

To achieve high-quality and reliable image generation, we generalize Inversion-DPO to two specific tasks: basic text-to-image generation and compositional image genera-

tion. Extensive experiments demonstrate the effectiveness of our method in both diffusion model training and inference, as well as its superior performance compared with current SOTA methods, achieving significant improvements in key evaluation metrics (mention the specific improvements, e.g., percentage gains). Figure 1 presents representative generated samples. Furthermore, we introduce a novel dataset with structural annotations and complex scene preference scores, enabling structured evaluation and deeper insight into Inversion-DPO’s compositional preference learning.

In summary, by leveraging the principles of DDIM inversion, we address the computational accuracy and efficiency limitations of DPO-based methods. The optimized diffusion model achieves state-of-the-art performance in both basic text-to-image and compositional image generation tasks.

## 2. Related Work

**Alignment of Diffusion Models.** As generative models are widely used, aligning outputs with user preferences has become a key focus. Researchers are integrating Reinforcement Learning from Human Feedback (RLHF) [2, 42] into diffusion models to improve controllability and accuracy. A common approach involves using pre-trained or additional reward models [8, 22, 28, 55, 72], leveraging human feedback and external signals to fine-tune generation. ImageReward [63] trains a reward model based on human feedback to improve image quality and semantic alignment. DPOK [11] and DDPO [3] combine reward signals with reinforcement learning for fine-tuning diffusion models, guiding generation through real-time feedback. ReNO [10] introduces a strategy that adjusts initial noise with reward signals, bypassing model training. IterComp [71] collects and combines model preferences, using iterative feedback to enhance generative capability.

The methods above typically require explicit training of reward models. Alternatively, some approaches bypass reward models and directly fine-tune generative models via reinforcement learning. [40] For example, Diffusion-DPO [57] simplifies training by using differentiable reward signals for end-to-end fine-tuning. D3PO [65] eliminates explicit reward model training by using human feedback to guide the process. A Dense Reward View [68] enhances reward fine-tuning with dense feedback at each denoising step, improving efficiency and stability. SPO [33] adjusts denoising performance at each step with a preference model and resampler. While these DPO-based methods reduce reward model overhead, they still face post-training challenges. Recent works have explored using inversion techniques to improve DPO for diffusion models. DDIM-InPO [37] employs a reparameterization approach that treats diffusion models as single-step generators, selectively

fine-tuning only the latent variables most correlated with preference data. SmPO-Diffusion [38] introduces smoothed preference distributions combined with a Renoise Inversion technique, performing multiple DDIM inversion steps followed by an additional renoise step to handle preference variability. In contrast, our Inversion-DPO directly leverages complete DDIM inversion to precisely compute the intractable posterior  $p_\theta(x_{1:T}|x_0)$ , eliminating the approximation errors inherent in previous methods and achieving a more efficient loss formulation with only two matching terms instead of four KL divergences, improving accuracy and efficiency.

**Compositional Image Generation.** Compositional Text-to-Image Generation is a challenge, especially when involving multiple objects and complex relationships [20, 67]. While many studies have improved generative models, the sequential text format still limits results, particularly in compositional image generation. Researchers have proposed methods to enhance control and spatial awareness. For instance, Compositional Diffusion [35] and Attend-and-Excite [5] improve generation efficiency but face limitations in complex scenes. Methods like GLIGEN [30] and Ranni [13] incorporate spatial conditioning and multimodal information to improve control, though they come with high training costs. BoxDiff [62] and RealCompo [70] optimize cross-attention and balance realism and complexity but remain dependent on bounding box accuracy. MIGC [74] and MIGC++ [73] address multi-instance composition using multimodal descriptions but focus on spatial control, failing to fully address abstract semantic relationships between objects.

To overcome the limitations of text formats, some studies have focused on using scene graphs for compositional generation [1, 15, 23, 35, 60, 67]. Scene graphs (SG) consist of nodes and edges representing objects and their relationships. Compositional SG2IM methods aim to generate high-quality images with multiple objects and complex relationships by better understanding and combining scene elements [12, 58, 61].

SGDiff [66] enhances scene graph-based image generation by pretraining a scene graph encoder and integrating it with Stable Diffusion. SG-Adapter [51] fine-tunes Stable Diffusion to incorporate scene graph information, improving image quality and semantic consistency. R3CD [34] introduces SG Transformers to expand diffusion models, learning abstract object interactions in larger datasets. DisCo [59] combines scene graph decomposition with VAEs and diffusion models for more diverse outputs. The LAION-SG dataset [31] further improves the model’s understanding of complex scenes.

Despite progress, compositional image generation still faces challenges in fidelity and efficiency. Our proposed method shows superior performance on difficult down-

stream tasks.

### 3. Preliminary

#### 3.1. Diffusion-DPO

Reinforcement Learning from Human Feedback (RLHF) typically involves two stages: training a reward model from pairwise preferences and optimizing policies via reinforcement learning (RL). Direct Preference Optimization (DPO) [45] bypasses this complexity by directly optimizing policies using preference data under a classification objective. Formally, given preference pairs  $(x_0^w, x_0^l)$  conditioned on prompts  $c$ , the Bradley-Terry model defines preference likelihood as:

$$p_{\text{BT}}(x_0^w \succ x_0^l | c) = \sigma(r(c, x_0^w) - r(c, x_0^l)), \quad (1)$$

Here  $r(\cdot, \cdot)$  is a reward function. Traditional RLHF maximizes the KL-regularized reward:

$$\max_{p_\theta} \mathbb{E}_{x_0 \sim p_\theta(x_0|c)} [r(c, x_0)] - \beta \mathbb{D}_{\text{KL}}[p_\theta(x_0|c) \| p_{\theta_0}(x_0|c)], \quad (2)$$

with  $p_\theta$  as the distribution to be optimized and  $p_{\theta_0}$  a reference distribution. DPO reparameterizes the optimal policy  $p_\theta^*$  as:

$$p_\theta^*(x_0|c) \propto p_{\theta_0}(x_0|c) \exp(r(c, x_0)/\beta). \quad (3)$$

Substituting this into the Bradley-Terry likelihood eliminates the reward function, yielding the DPO loss:

$$\mathcal{L}_{\text{DPO}} = -\mathbb{E}_{(c, x_0^w, x_0^l)} \left[ \log \sigma \left( \beta \log \frac{p_\theta(x_0^w|c)}{p_{\theta_0}(x_0^w|c)} - \beta \log \frac{p_\theta(x_0^l|c)}{p_{\theta_0}(x_0^l|c)} \right) \right]. \quad (4)$$

This implicitly optimizes rewards while maintaining policy proximity to  $p_{\theta_0}$ , avoiding explicit reward modeling and RL instability.

For diffusion models, the challenge lies in defining likelihoods over generated images  $x_0$ . Diffusion-DPO [57] extends DPO by leveraging the evidence lower bound (ELBO) of diffusion processes. The KL-regularized reward maximization objective becomes:

$$\max_{p_\theta} \mathbb{E}_{p_\theta(x_{1:T}|c, x_0)} [R(c, x_{0:T})] - \beta \mathbb{D}_{\text{KL}}[p_\theta(x_{0:T}|c) \| p_{\theta_0}(x_{0:T}|c)], \quad (5)$$

Here  $R(c, x_{0:T})$  denotes the reward over the full diffusion trajectory. Given a winning or losing sample  $x_0$ , a posterior sampling  $p_\theta(x_{1:T}|x_0, c)$  is required to gain the noisy sample sequence  $x_{1:T}$  of  $p_\theta$ , which is intractable. By approximating the reverse process with the forward process  $q(x_{1:T}|x_0)$ , the loss simplifies to:

$$\begin{aligned} \mathcal{L}_{\text{Diffusion-DPO}} = & -\mathbb{E}_{(x_0^w, x_0^l), t, q(x_t^w|x_0^w), q(x_t^l|x_0^l)} \log \sigma(-\beta T \omega(\lambda_t) ( \\ & \|\epsilon^w - \epsilon_\theta(x_t^w, t)\|_2^2 - \|\epsilon^w - \epsilon_{\theta_0}(x_t^w, t)\|_2^2 - \\ & (\|\epsilon^l - \epsilon_\theta(x_t^l, t)\|_2^2 - \|\epsilon^l - \epsilon_{\theta_0}(x_t^l, t)\|_2^2))), \end{aligned} \quad (6)$$

Here  $\epsilon_\theta$  is the denoising network,  $\epsilon_{\theta_0}$  the pretrained network, and  $\omega(\lambda_t)$  absorbs all coefficients. This formulation improves  $\epsilon_\theta$  on denoising of preferred samples  $x_0^w$  more than dispreferred  $x_0^l$ , aligning diffusion models with preferences without additional inference costs or mode collapse.

### 3.2. DDIM Inversion

In this part, we introduce DDIM Inversion which is crucial in our proposed method. In traditional diffusion models like DDPM [17], the generative process starts with Gaussian noise  $x_T$  and gradually denoises through a reverse Markov chain to obtain a clean image  $x_0$ . Although the training procedure maximizes a variational lower bound, the sampling process is inherently stochastic, making it difficult to precisely recover the sampling path  $\{x_t\}$  for a given  $x_0$ .

Denoising Diffusion Implicit Models (DDIM) [52] proposes a non-Markovian inference process. Given any intermediate state  $x_t$ , the trained  $\epsilon_\theta(x_t, t)$  estimates the corresponding denoised sample:

$$\hat{x}_0 = f_\theta^{(t)}(x_t) = \frac{x_t - \sqrt{1 - \alpha_t} \epsilon_\theta(x_t, t)}{\sqrt{\alpha_t}}, \quad (7)$$

where  $\alpha_t$  is a signal retention coefficient associated with time step  $t$ . When  $t > 1$ , the generative process is given by

$$p_\theta(x_{t-1}|x_t) = \mathcal{N}(\sqrt{\alpha_{t-1}}\hat{x}_0 + \sqrt{1 - \alpha_{t-1} - \sigma_t^2} \cdot \frac{x_t - \sqrt{\alpha_t}\hat{x}_0}{\sqrt{1 - \alpha_t}}, \sigma_t^2 \mathbf{I}) \quad (8)$$

When  $t = 1$ ,  $p_\theta(x_0|x_1) = \mathcal{N}(\hat{x}_0, \sigma_1^2 \mathbf{I})$ . The noise term  $\sigma_t$  can be zero during sampling, thus converting the generative process into a deterministic implicit probabilistic model. Since the update process no longer introduces additional randomness, DDIM not only allows high-quality samples to be generated in fewer steps but also renders the generative mapping invertible, which enables recovering the sampling trajectory  $\{x_1, x_2, \dots, x_T\}$  from  $x_0$  [52].

It has been observed that when the number of sampling steps is large, predicted noises are close in adjacent steps [75]. This supports the assumption that the ordinary differential equation (ODE) process can be reversed within the limit of small steps [25], which means  $\epsilon_\theta(x_t, t) \approx \epsilon_\theta(x_{t-1}, t-1)$ . This key property allows us to invert the DDIM generative process [9, 24]. Starting from a real sample  $x_0$ , we can backtrack to sampling its potential denoising sequence  $\{x_1, x_2, \dots, x_T\}$ . The detailed inversion iteration is

$$x_t = \sqrt{\frac{\alpha_t}{\alpha_{t-1}}} x_{t-1} + (\sqrt{1 - \alpha_t} - \sqrt{\frac{\alpha_t}{\alpha_{t-1}}} - \alpha_t) \epsilon_\theta(x_{t-1}, t-1) \quad (9)$$

Such iteration finally reaches  $x_T$ . Under the assumption above, with  $x_T$  as the initial noise, a deterministic sampling

process  $\epsilon_\theta$  is likely to recover the sequence  $\{x_{T-1}, \dots, x_1\}$  and come back to the original  $x_0$ . More advanced estimations [14, 24] give more precise recovery. This capability to recover the latent path from  $x_0$  provides a theoretical basis for Inversion-DPO we introduce next.

## 4. method

### 4.1. Inversion Direct Preference Optimization

DPO [45] is an effective reward-guided post-training approach that directly learns human preferences through a reparameterized policy, rather than optimizing a reward function and then performing reinforcement learning (RL).

Recall that when adapting DPO to diffusion models [57], the objective shifts from fitting  $x_0$  to fitting the trajectory  $(x_0, \dots, x_T)$  with

$$\mathcal{L}_{\text{Diffusion-DPO}}(\theta) = -\mathbb{E}_{(x_0^w, x_0^l)} \log \sigma \left( \beta \mathbb{E}_{\substack{x_{1:T}^w \sim p_\theta(x_{1:T}^w | x_0^w) \\ x_{1:T}^l \sim p_\theta(x_{1:T}^l | x_0^l)}} \left[ \log \frac{p_\theta(x_{0:T}^w)}{p_{\theta_0}(x_{0:T}^w)} - \log \frac{p_\theta(x_{0:T}^l)}{p_{\theta_0}(x_{0:T}^l)} \right] \right) \quad (10)$$

To optimize this,  $x_{1:T}$  across all time steps are required with a posterior sampling of  $p_\theta$ . Thus, Diffusion-DPO encounters two key limitations: 1) The intractability of  $p_\theta(x_{1:T}|x_0)$  results in a substitution with  $q(x_{1:T}|x_0)$  as approximation, introducing large estimation errors; 2) The KL-Divergence formulation expands the original pairwise comparison into four terms.

We address these issues by designing Inversion-DPO (Fig. 2). Our key insight stems from the deterministic characteristic of DDIM Inversion [52]. Given a sample  $x_0$ , DDIM Inversion constructs the sampling trajectory  $x_{1:T}$  leading to  $x_0$  through a deterministic mapping by equation (9). Thus, we propose to approximate the posterior  $p_\theta(x_{1:T}|x_0)$  with DDIM inversion. This eliminates the need for stochastic approximation  $q$  in trajectory estimation. Using DDIM Inversion is reasonable with three advantages. First, assuming the deterministic sampling setting, the posterior inference is the inversion process. Thus, the resulting  $x_{1:T}$  are more precise. Second, such inversion is compatible with the definition of the reward function on diffusion in equation (5), so the implicit reward learning is also precise. Third, the final estimated expectation in (10) is also more precise in this case.

Given the  $x_{1:T}^w$ , we derive the following computation within the expectation. Specifically,  $\log \frac{p_\theta(x_{0:T}^w)}{p_{\theta_0}(x_{0:T}^w)}$  is first decomposed into the differences in conditional probabilities at each time step:

$$\log \frac{p_\theta(x_{0:T}^w)}{p_{\theta_0}(x_{0:T}^w)} = \sum_{t=1}^T [\log p_\theta(x_{t-1}^w | x_t^w) - \log p_{\theta_0}(x_{t-1}^w | x_t^w)] \quad (11)$$

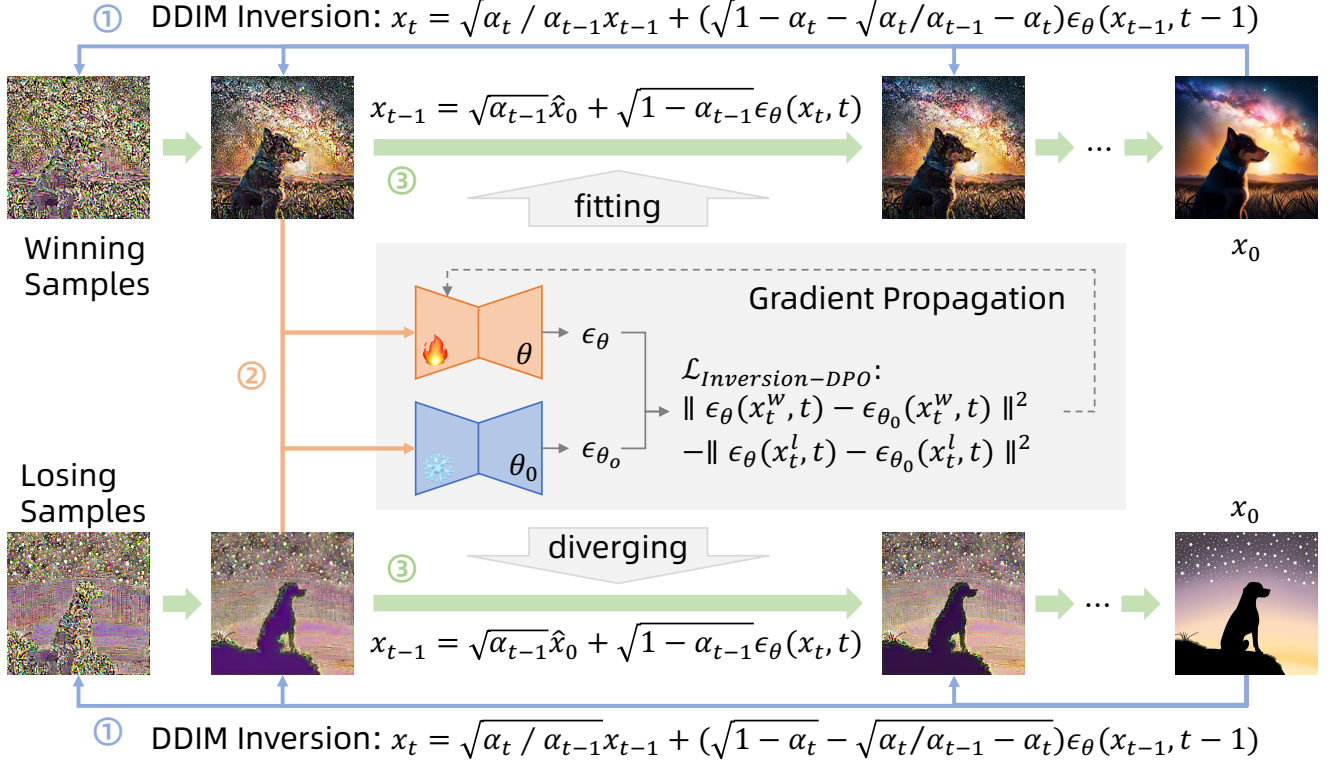


Figure 2. Computation pipeline of the proposed Inversion-DPO. 1) Given an initial image  $x_0$ , we obtain the diffusion trajectories  $\{x_1, x_2, \dots, x_T\}$  of both the winning and losing samples from a reference model via DDIM inversion. 2) At each timestep along the diffusion trajectory, the model is trained to predict the noise  $\epsilon$ , aligning it closely with the  $\epsilon$  of the winning sample while diverging from that of the losing sample. 3) This process is repeated across the entire diffusion trajectory, continuously updating model parameters until the final predicted image is generated.

Since  $p_\theta$  and  $p_{\theta_0}$  share the same distribution of  $x_T$  as standard Gaussian,  $\log p_\theta(x_T^w) - \log p_{\theta_0}(x_T^w)$  cancel out. The conditional probabilities of  $p_\theta$  and  $p_{\theta_0}$  are Gaussian distributions as in equation (8) and becomes dirac-delta as  $\sigma_t$  approaches 0. We first continue derivation with  $\sigma_t \neq 0$  and adopt a simple approximation [17] of the final loss.

Given the assumption of inversion in Sec. 3.2, the values of  $x_{t-1}^w$  are similar in the inversion from  $x_0^w$  and in the sampling from  $x_T^w$ . Therefore,  $\log p_\theta(x_{t-1}^w | x_t^w)$  is only related to  $\sigma_t^2$  and thus constant. At the same time, given

$$\mu_{\theta_0}(x_t^w) = \frac{\sqrt{\alpha_{t-1}}}{\sqrt{\alpha_t}} x_t^w + \quad (12)$$

$$\left( \sqrt{1 - \alpha_{t-1} - \sigma_t^2} - \frac{\sqrt{\alpha_{t-1}(1 - \alpha_t)}}{\sqrt{\alpha_t}} \right) \epsilon_{\theta_0}(x_t^w, t) \quad (13)$$

we have the following (details included in supplementary material):

$$\begin{aligned} -\log p_{\theta_0}(x_{t-1}^w | x_t^w) &\propto \|\mu_{\theta_0}(x_t^w) - x_{t-1}^w\|^2 \\ &\propto \|\epsilon_{\theta_0}(x_t^w, t) - \epsilon_\theta(x_t^w, t)\|^2 \end{aligned} \quad (14)$$

Summing the contributions across all time steps, we can arrive at:

$$\log \frac{p_\theta(\mathbf{x}_{0:T}^w)}{p_{\theta_0}(\mathbf{x}_{0:T}^w)} \propto \left[ \sum_{t=1}^T \|\epsilon_\theta(x_t^w, t) - \epsilon_{\theta_0}(x_t^w, t)\|^2 \right], \quad (15)$$

The term for the losing sample in equation (10) is derived analogously. Each term in the objective can be computed exactly. The log-probability ratio now directly captures the policy divergence without introducing approximation errors.

Taking all together, the final objective becomes:

$$\begin{aligned} \mathcal{L}_{\text{Inversion-DPO}}(\theta) &= -\mathbb{E}_{(x_0^w, x_0^l)} \log \sigma \left( \beta \mathbb{E}_{\substack{\mathbf{x}_{1:T}^w \sim p_\theta(\mathbf{x}_{1:T}^w | \mathbf{x}_0^w) \\ \mathbf{x}_{1:T}^l \sim p_\theta(\mathbf{x}_{1:T}^l | \mathbf{x}_0^l)}} \right) \\ &\sum_{t=1}^T \left[ \|\epsilon_\theta(x_t^w, t) - \epsilon_{\theta_0}(x_t^w, t)\|^2 - \|\epsilon_\theta(x_t^l, t) - \epsilon_{\theta_0}(x_t^l, t)\|^2 \right] \end{aligned} \quad (16)$$

Notably, during the training of Inversion-DPO, the previous four-term loss collapses into two deterministic summations due to trajectory determinism, which is conceptually simpler. This simplification also yields non-negligible

improvements in optimization efficiency for model training. The pretrained  $\epsilon_{\theta_0}$  can be transformed to approximate the score. Fitting the noise added as in (6) introduces extra variance [41, 56] which is unstable in the training [64], while fitting the predicted noise close to the score is more stable and thus improves the training efficiency. Our training schema fundamentally resolves the precision-efficiency tradeoff in preference-based diffusion alignment.

## 4.2. Inversion-DPO with multiple objectives

For effective Inversion-DPO training, both positive (i.e., winning samples) and negative (i.e., losing samples) data pairs are required to guide the optimization. While manual annotation is commonly used to obtain such pairs [57, 71], it is costly and prone to ambiguity. To address this, recent works [3, 39, 54, 65] adopt automatic metrics to rank images as guidance. We follow this strategy. However, relying on a single metric is often inadequate to comprehensively capture the quality of the outputs, especially in complex scene generation scenarios. Therefore, we introduce a multi-objective learning strategy, leveraging multiple metrics to provide more reliable and informative preference signals.

Specifically, we incorporate multiple evaluation metrics to derive the reward scores for data pairs, computed as follows:

$$r(c, x_0) = \frac{1}{N} \sum_{i=1}^N r_i(c, x_0) \quad (17)$$

Here,  $N$  denotes the number of evaluation metrics utilized in the current task, and  $(c, x_0)$  represents the conditional sample pair generated by  $p_{\theta_0}$  given the condition  $c$ .

We evaluate the effectiveness of Inversion-DPO in two representative tasks. In addition to the typical text-to-image generation, we further assess it in the more challenging setting of compositional image generation, which requires the model to accurately synthesize complex scenes involving multiple objects and relationships. Existing studies [31, 59] suggest that, compared to textual annotations, structured annotations provide a more compact and explicit form of information integration, making them more effective for representing complex scenes. Such structured annotations are typically represented as graphs, consisting of nodes and edges that denote objects in the scene and their interactions, respectively.

On basic text-to-image tasks, Pick-a-Pic dataset [26] serves as a reliable source of supervision for training Inversion-DPO. However, for compositional generation, there is a lack of corresponding paired datasets that can be directly utilized. This is because existing datasets with structured annotations [4, 27, 31] provide only single-condition samples, making them insufficient for preference-based learning. To bridge this gap, we construct a paired

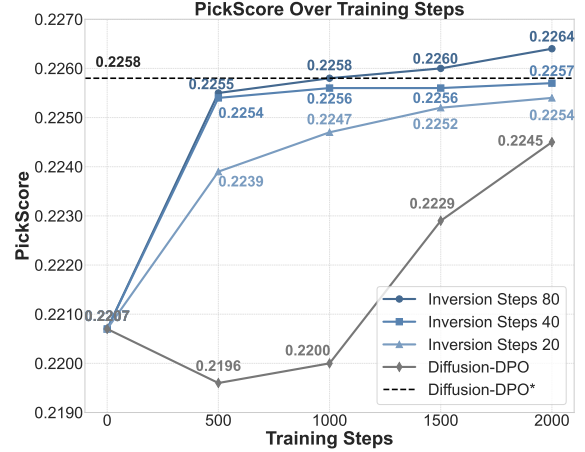


Figure 3. A demonstration of how PickScore increase with more training steps. The blue curve shows the performance of our Inversion-DPO trained with different numbers of DDIM inversion steps. The gray curve represents our retraining with the official implementation of Diffusion-DPO [57], while the dashed line corresponds to the officially released weights. Our model with 80-step inversion outperforms the both the retraining and the released Diffusion-DPO checkpoint. All models are trained under identical configurations.

dataset with structured annotations to support alignment and evaluation.

In detail, for a given complex scene annotation, we generate four samples using an existing baseline [31], and compute a multi-dimensional score for each generated image. During training, the model determines positive and negative samples based on a combination of these scores, guiding the learning of Inversion-DPO.

To ensure effective evaluation of complex scene images, we adopt two representative metrics—DPG-Bench Score [18] and the 3-in-1 score from T2I-CompBench [19]—as the criteria for multi-objective learning. In total, we generate 11,140 images for 2,785 annotations, with each image associated with a comprehensive complex scene score. Rather than enforcing fixed pairwise bindings, we allow the model to dynamically determine relative “winning” and “losing” samples based on their comprehensive scores during training. This approach prevents the dataset size from being constrained to the original 2,785 samples, enabling scalable data expansion within a certain range and ultimately improving training quality.

## 5. Experiments

### 5.1. Dataset and Implementation Details

**Dataset.** We use the Pick-a-Pic v2 dataset [26] to train our T2I model, which contains paired preferences of images generated by SDXL-beta and Dreamlike, along with

prompts and preference pairs collected from the web. Following the same data processing approach as Diffusion-DPO [57], we exclud 12% of tie samples, ultimately obtaining 851,293 effective data pairs. For the compositional image generation task, as described in Section 4.2, we curate compositional image pairs from LAION-SG [31] for training, ensuring data quality and diversity.

**Training.** During the training process, we employ the Adafactor [50] optimizer for SDXL and SGXL-SG to save memory, while AdamW [36] was used for SD1.5 training. The learning rate for all models was uniformly set to  $1e-6$ . Specifically, the  $\beta$  parameter in Inversion-DPO was set to 2000. We also set the Inversion Steps to 20, 40, and 80, respectively, to observe the impact of different DDIM Inversion steps on model performance, which is detailed in our ablation study. Each model was trained for 2000 steps, with all training tasks completed on two NVIDIA H800 GPUs.

## 5.2. Baselines and Evaluation Metrics

For the typical text-to-image generation task, we evaluate a set of representative baseline models and post-training methods, including SD1.5 [47], SDXL [43], Diffusion-DPO [57], DDPO [3], D3PO [65], Demon [69], and IterComp [71]. The generated results are assessed using PickScore [26], CLIP Score [44], and Aesthetic Score [49], which respectively measure alignment with human preference, semantic consistency with the input prompt, and the aesthetic quality of image details.

For compositional image generation, we evaluate SGDiff [66], SG-Adapter [51], SDXL-SG [31], and SD1.5-SG [31]. Considering the objectives of complex scene generation, we adopt FID [16] as the image quality metric, along with SG-IoU, Entity-IoU, and Relation-IoU [51], which respectively assess scene-level consistency, object-level consistency, and the consistency of relationships between objects within the generated images.

## 5.3. Qualitative Results

Figure 1 illustrates the visual performance of our Inversion-DPO compared to baseline models on text-to-image tasks. Each row shows an input prompt and the corresponding generated images. Compared to existing baselines [3, 43, 57, 69], Inversion-DPO exhibits higher visual appeal and achieves higher PickScore. Moreover, in Fig. 4, our method demonstrates promising potential in controlling fine-grained detail generation, which is a persistent challenge for text-to-image models. We further visualize results on more challenging compositional image generation tasks. As shown in Fig. 5, Inversion-DPO demonstrates superior performance in terms of object occurrence, relation accuracy, and attribute binding.

We also conduct a user study, and Inversion-DPO enjoys 66.53% human preference compared to SDXL and 72.67%

Method	PickScore <sup>†</sup>	CLIP <sup>†</sup>	Aesthetic <sup>†</sup>
SDXL [43]	0.223	0.334	6.07
Diffusion-DPO [57]	0.227	0.340	6.05
DDPO [3]	0.222	0.336	6.10
D3PO [65]	0.223	0.338	5.99
Demon [69]	0.220	0.336	6.15
IterComp [71]	<b>0.232</b>	0.340	6.22
<b>Inversion-DPO</b>	<b>0.232</b>	<b>0.341</b>	<b>6.24</b>
SD1.5 [47]	0.207	0.320	5.61
Diffusion-DPO <sup>†</sup>	<b>0.212</b>	0.324	5.73
<b>Inversion-DPO<sup>†</sup></b>	<b>0.212</b>	<b>0.325</b>	<b>5.74</b>

Table 1. Quantitative results of typical text-to-image generation. <sup>†</sup> indicates that the model is built upon SD1.5. The same applies to the following tables.

Method	FID <sup>↓</sup>	SG-IoU <sup>↑</sup>	Ent.-IoU <sup>↑</sup>	Rel.-IoU <sup>↑</sup>
SGDiff [66]	35.8	0.304	0.787	0.698
SG-Adapter [51]	27.8	0.314	0.771	0.693
R3CD [34]	27.0	0.342	0.803	0.715
SDXL-SG [31]	26.7	0.340	0.792	0.703
<b>Inversion-DPO*</b>	<b>25.1</b>	<b>0.354</b>	<b>0.830</b>	<b>0.739</b>
SD1.5-SG	56.3	0.179	0.614	0.530
<b>Inversion-DPO<sup>†</sup>*</b>	<b>54.9</b>	<b>0.184</b>	<b>0.624</b>	<b>0.565</b>

Table 2. Quantitative results on the more challenging task of compositional image generation. \* means the results of Inversion-DPO trained on the compositional paired dataset.

versus Diffusion-DPO. More details are in supplementary material.

## 5.4. Quantitative Results

Table 1 reports the quantitative performance on typical text-to-image generation for both baseline models and ours. Compared to base T2I models [43, 47], post-training methods [3, 57, 65, 71], and training-free approach [69], Inversion-DPO achieves state-of-the-art results in terms of human preference alignment (PickScore), text-image consistency (CLIP Score), and aesthetic quality (Aesthetic Score). In addition to the formal SDXL-based version of Inversion-DPO, we also validate its adaptability on SD1.5.

We further investigate the performance of the proposed method on compositional image generation. As in Tab. 2, after fine-tuning on the compositional dataset, Inversion-DPO achieves the best image quality as measured by FID, outperforming existing baseline models. Moreover, it obtains the highest scores on complexity evaluation metrics, which comprehensively assess the fidelity of the generated images at the scene, entity, and relation levels.

Empirically, our method also brings notable improve-

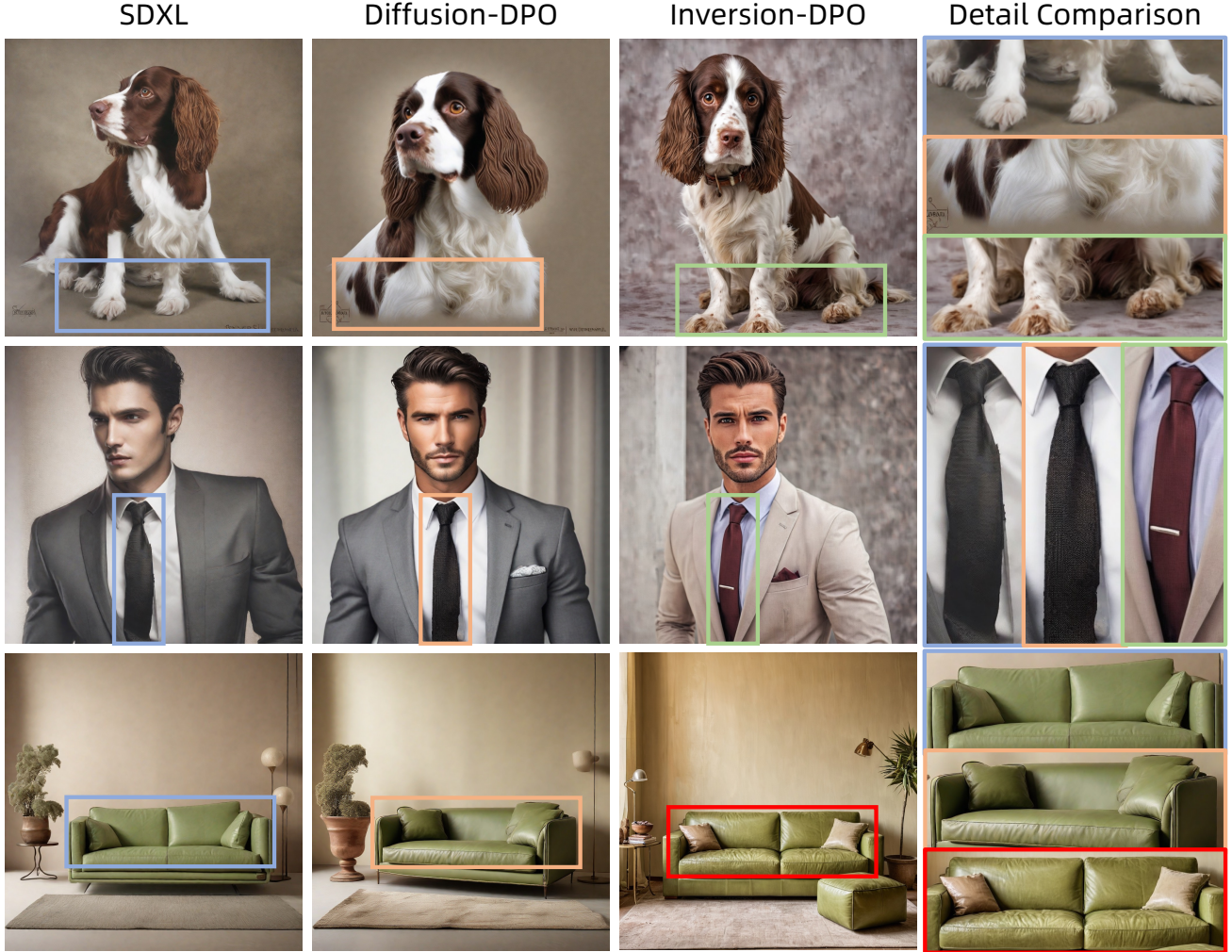


Figure 4. A comparison of generation details. Existing models often struggle to produce fine-grained details, while Inversion-DPO demonstrates a higher level of fidelity in generating nuanced elements such as limbs, ties, and textures.

ments in training efficiency. In Fig. 3, Inversion-DPO achieves superior performance with significantly fewer training steps compared to Diffusion-DPO. Due to hardware limitation, our reimplementation of Diffusion-DPO with the official implementation does match the performance of the official checkpoint. Besides, we observe a slight decay of performance at the beginning which may be a result of the instability of Diffusion-DPO’s training. Nevertheless, under the same resources, our Inversion-DPO constantly improves the performance of the generative model. Specifically, our variants with only 20-step DDIM Inversion reaches a performance of 0.2247 at 1000 steps, comparable to Diffusion-DPO’s 0.2245 at 2000, over  $2\times$  faster. Inversion-DPO with 80 steps is over  $4\times$  faster. Furthermore, at 2000 steps Inversion-DPO with 80-step inversion also outperforms the reported performance of Diffusion-DPO as labeled by the

# Inversion Steps	PickScore <sup>↑</sup>	CLIP <sup>↑</sup>	Aesthetic <sup>↑</sup>
20	0.228	0.340	6.08
40	0.229	0.341	6.13
80	<b>0.232</b>	<b>0.341</b>	<b>6.24</b>

Table 3. Effect of inversion steps on model performance.

dotted line, further demonstrating the advantages of our method in both precision and efficiency. Results on other metrics are in Supplementary Material.

### 5.5. Ablation Study

**Analysis of the different inversion steps.** We analyze the impact of different DDIM inversion steps on model training, with results shown in Tab. 3 and Fig. 3. It is evident

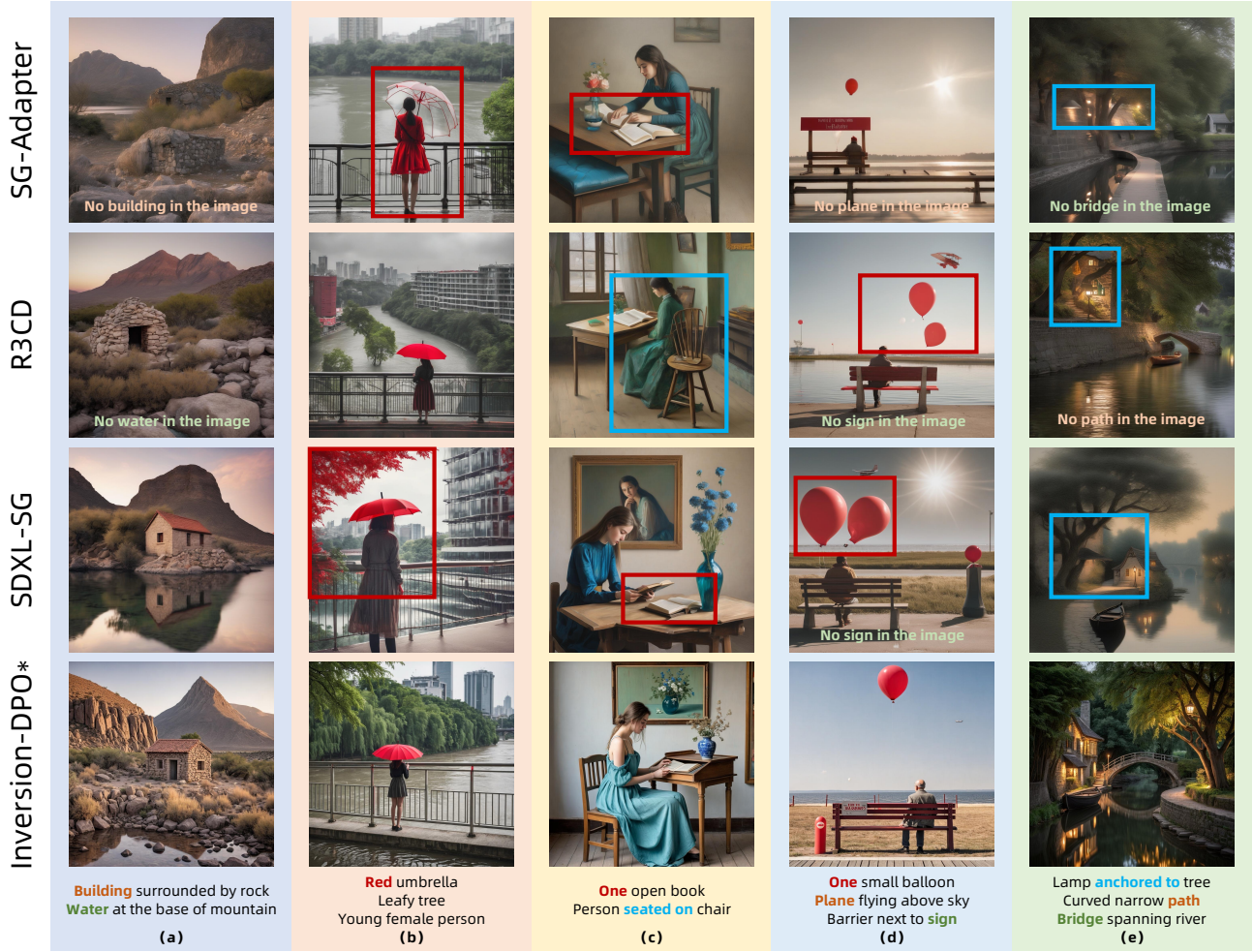


Figure 5. Qualitative results on compositional image generation. Inversion-DPO proves effective in addressing key challenges in compositional image generation, including object omission (orange and green annotations in (a), (d), and (e)), attribute errors (red annotations in (b), (c), and (d)), and relation inaccuracies (blue annotations in (c) and (d)). As shown in the last row, Inversion-DPO achieves satisfactory generation results on cases where baseline models struggle.

that as the number of inversion steps increases, the model consistently achieves better performance across all metrics. This can be attributed to the fact that with more DDIM inversion steps, the distributional gap between adjacent steps becomes smaller, satisfying the assumption in Sec. 3.2 and making it easier to guide the model toward correct optimization directions. The configuration with 80 inversion steps is ultimately selected for training Inversion-DPO for a balance between performance and computational cost.

## 6. Conclusion

We presents Inversion-DPO, a novel post-training framework that integrates DDIM Inversion with DPO to achieve efficient and precise alignment in diffusion models. By leveraging the deterministic trajectory recovery of

DDIM inversion, our method reduces approximation errors, achieving more than  $2\times$  training acceleration. A multi-objective scoring strategy further enhances robustness in compositional image generation. Inversion-DPO achieves SOTA performance on both text-to-image generation and compositional image generation. We additionally curate a structured dataset of 11,140 annotated images to support complex scene synthesis.

## References

- [1] Oron Ashual and Lior Wolf. Specifying object attributes and relations in interactive scene generation. pages 4560–4568, 2019. 3
- [2] Yuntao Bai, Andy Jones, Kamal Ndousse, Amanda Askell, Anna Chen, Nova DasSarma, Dawn Drain, Stanislav Fort, Deep Ganguli, Tom Henighan, Nicholas Joseph, Saurav Ka-

- davath, Jackson Kernion, Tom Conerly, Sheer El-Showk, Nelson Elhage, Zac Hatfield-Dodds, Danny Hernandez, Tristan Hume, Scott Johnston, Shauna Kravec, Liane Lovitt, Neel Nanda, Catherine Olsson, Dario Amodei, Tom Brown, Jack Clark, Sam McCandlish, Chris Olah, Ben Mann, and Jared Kaplan. Training a helpful and harmless assistant with reinforcement learning from human feedback. *ArXiv*, abs/2204.05862, 2022. 2
- [3] Kevin Black, Michael Janner, Yilun Du, Ilya Kostrikov, and Sergey Levine. Training diffusion models with reinforcement learning. *ArXiv*, abs/2305.13301, 2024. 2, 6, 7
- [4] Holger Caesar, Jasper Uijlings, and Vittorio Ferrari. Cocostuff: Thing and stuff classes in context. pages 1209–1218, 2018. 6
- [5] Hila Chefer, Yuval Alaluf, Yael Vinker, Lior Wolf, and Daniel Cohen-Or. Attend-and-excite: Attention-based semantic guidance for text-to-image diffusion models. *ACM Trans. Graph.*, 42(4), 2023. 3
- [6] Junsong Chen, Chongjian Ge, Enze Xie, Yue Wu, Lewei Yao, Xiaozhe Ren, Zhongdao Wang, Ping Luo, Huchuan Lu, and Zhenguo Li. Pixart- $\sigma$ : Weak-to-strong training of diffusion transformer for 4k text-to-image generation. *ArXiv*, abs/2403.04692, 2024. 2
- [7] Prafulla Dhariwal and Alexander Nichol. Diffusion models beat gans on image synthesis. In *Advances in Neural Information Processing Systems*, pages 8780–8794, 2021. 2
- [8] Carles Domingo-Enrich, Michal Drozdal, Brian Karrer, and Ricky T. Q. Chen. Adjoint matching: Fine-tuning flow and diffusion generative models with memoryless stochastic optimal control. *ArXiv*, abs/2409.08861, 2025. 2
- [9] Wenkai Dong, Song Xue, Xiaoyue Duan, and Shumin Han. Prompt tuning inversion for text-driven image editing using diffusion models. In *2023 IEEE/CVF International Conference on Computer Vision (ICCV)*, pages 7396–7406, 2023. 4
- [10] Luca Eyring, Shyamgopal Karthik, Karsten Roth, Alexey Dosovitskiy, and Zeynep Akata. Reno: Enhancing one-step text-to-image models through reward-based noise optimization. In *Advances in Neural Information Processing Systems*, pages 125487–125519. Curran Associates, Inc., 2024. 2
- [11] Ying Fan, Olivia Watkins, Yuqing Du, Hao Liu, Moonkyung Ryu, Craig Boutilier, Pieter Abbeel, Mohammad Ghavamzadeh, Kangwook Lee, and Kimin Lee. Dpok: Reinforcement learning for fine-tuning text-to-image diffusion models. In *Advances in Neural Information Processing Systems*, pages 79858–79885. Curran Associates, Inc., 2023. 2
- [12] Weixi Feng, Xuehai He, Tsu-Jui Fu, Varun Jampani, Arjun Akula, Pradyumna Narayana, Sugato Basu, Xin Eric Wang, and William Yang Wang. Training-free structured diffusion guidance for compositional text-to-image synthesis. 2023. 3
- [13] Yutong Feng, Biao Gong, Di Chen, Yujun Shen, Yu Liu, and Jingren Zhou. Ranni: Taming text-to-image diffusion for accurate instruction following. pages 4744–4753, 2024. 3
- [14] Daniel Garibi, Or Patashnik, Andrey Voynov, Hadar Averbuch-Elor, and Daniel Cohen-Or. Renoise: Real image inversion through iterative noising. In *Computer Vision – ECCV 2024*, pages 395–413, Cham, 2025. Springer Nature Switzerland. 4
- [15] Xuan Han, Yihao Zhao, and Mingyu You. Scene diffusion: Text-driven scene image synthesis conditioning on a single 3d model. In *Proceedings of the 32nd ACM International Conference on Multimedia*, page 7862–7870. Association for Computing Machinery, 2024. 3
- [16] Martin Heusel, Hubert Ramsauer, Thomas Unterthiner, Bernhard Nessler, Günter Klambauer, and Sepp Hochreiter. Gans trained by a two time-scale update rule converge to a nash equilibrium. *ArXiv*, abs/1706.08500, 2017. 7
- [17] Jonathan Ho, Ajay Jain, and Pieter Abbeel. Denoising diffusion probabilistic models. In *Advances in Neural Information Processing Systems*, pages 6840–6851, 2020. 4, 5, 15, 16
- [18] Xiwei Hu, Rui Wang, Yixiao Fang, Bin Fu, Pei Cheng, and Gang Yu. Ella: Equip diffusion models with llm for enhanced semantic alignment, 2024. 6
- [19] Kaiyi Huang, Kaiyue Sun, Enze Xie, Zhenguo Li, and Xi-hui Liu. T2i-compbench: A comprehensive benchmark for open-world compositional text-to-image generation. In *Advances in Neural Information Processing Systems*, pages 78723–78747, 2023. 6
- [20] Yiheng Huang, Hui Yang, Chuanchen Luo, Yuxi Wang, Shibiao Xu, Zhaoxiang Zhang, Man Zhang, and Junran Peng. Stablemofusion: Towards robust and efficient diffusion-based motion generation framework. In *Proceedings of the 32nd ACM International Conference on Multimedia*, page 224–232. Association for Computing Machinery, 2024. 3
- [21] Yangqin Jiang, Lianghao Xia, Wei Wei, Da Luo, Kangyi Lin, and Chao Huang. Diffmm: Multi-modal diffusion model for recommendation. In *Proceedings of the 32nd ACM International Conference on Multimedia*, page 7591–7599. Association for Computing Machinery, 2024. 2
- [22] Zutao Jiang, Guian Fang, Jianhua Han, Guansong Lu, Hang Xu, Shengcai Liao, Xiaojun Chang, and Xiaodan Liang. Realigndiff: Boosting text-to-image diffusion model with coarse-to-fine semantic re-alignment. *ArXiv*, abs/2305.19599, 2024. 2
- [23] Justin Johnson, Agrim Gupta, and Li Fei-Fei. Image generation from scene graphs. pages 1219–1228, 2018. 3
- [24] Xuan Ju, Ailing Zeng, Yuxuan Bian, Shaoteng Liu, and Qiang Xu. Direct inversion: Boosting diffusion-based editing with 3 lines of code. In *International Conference on Representation Learning*, 2023. 4
- [25] Gwanghyun Kim, Taesung Kwon, and Jong Chul Ye. Diffusionclip: Text-guided diffusion models for robust image manipulation. In *2022 IEEE/CVF Conference on Computer Vision and Pattern Recognition (CVPR)*, pages 2416–2425, 2022. 4
- [26] Yuval Kirstain, Adam Polyak, Uriel Singer, Shahbuland Matiana, Joe Penna, and Omer Levy. Pick-a-pic: An open dataset of user preferences for text-to-image generation. In *Advances in Neural Information Processing Systems*, pages 36652–36663, 2023. 6, 7, 14

- [27] Ranjay Krishna, Yuke Zhu, Oliver Groth, Justin Johnson, Kenji Hata, Joshua Kravitz, Stephanie Chen, Yannis Kalantidis, Li-Jia Li, David A Shamma, et al. Visual genome: Connecting language and vision using crowdsourced dense image annotations. *International Journal of Computer Vision*, 123(1):32–73, 2017. [6](#)
- [28] Jiachen Li, Weixi Feng, Wenhui Chen, and William Yang Wang. Reward guided latent consistency distillation. *Transactions on Machine Learning Research*, 2024. Featured Certification. [2](#)
- [29] Peiming Li, Ziyi Wang, Mengyuan Liu, Hong Liu, and Chen Chen. Clickdiff: Click to induce semantic contact map for controllable grasp generation with diffusion models. In *Proceedings of the 32nd ACM International Conference on Multimedia*, page 273–281. Association for Computing Machinery, 2024. [2](#)
- [30] Yuheng Li, Haotian Liu, Qingyang Wu, Fangzhou Mu, Jianwei Yang, Jianfeng Gao, Chunyuan Li, and Yong Jae Lee. Gligen: Open-set grounded text-to-image generation. pages 22511–22521, 2023. [3](#)
- [31] Zejian Li, Chenye Meng, Yize Li, Ling Yang, Shengyuan Zhang, Jiarui Ma, Jiayi Li, Guang Yang, Changyuan Yang, Zhiyuan Yang, Jinxiong Chang, and Lingyun Sun. Laion-sg: An enhanced large-scale dataset for training complex image-text models with structural annotations. *ArXiv*, abs/2412.08580, 2024. [3](#), [6](#), [7](#)
- [32] Zhengqi Li, Richard Tucker, Noah Snively, and Aleksander Holynski. Generative image dynamics. pages 24142–24153, 2024. [2](#)
- [33] Zhanhao Liang, Yuhui Yuan, Shuyang Gu, Bohan Chen, Tiankai Hang, Mingxi Cheng, Ji Li, and Liang Zheng. Aesthetic post-training diffusion models from generic preferences with step-by-step preference optimization. *ArXiv*, abs/2406.04314, 2025. [2](#)
- [34] Jinxiu Liu and Qi Liu. R3cd: Scene graph to image generation with relation-aware compositional contrastive control diffusion. pages 3657–3665, 2024. [3](#), [7](#)
- [35] Nan Liu, Shuang Li, Yilun Du, Antonio Torralba, and Joshua B. Tenenbaum. Compositional visual generation with composable diffusion models. In *European Conference on Computer Vision*, pages 423–439, 2022. [3](#)
- [36] Ilya Loshchilov and Frank Hutter. Decoupled weight decay regularization, 2019. [7](#)
- [37] Yunhong Lu, Qichao Wang, Hengyuan Cao, Xierui Wang, Xiaoyin Xu, and Min Zhang. Inpo: Inversion preference optimization with reparametrized ddim for efficient diffusion model alignment, 2025. [2](#)
- [38] Yunhong Lu, Qichao Wang, Hengyuan Cao, Xiaoyin Xu, and Min Zhang. Smoothed preference optimization via renoise inversion for aligning diffusion models with varied human preferences, 2025. [3](#)
- [39] Nanye Ma, Shangyuan Tong, Haolin Jia, Hexiang Hu, Yuchuan Su, Mingda Zhang, Xuan Yang, Yandong Li, Tommi Jaakkola, Xuhui Jia, and Saining Xie. Inference-time scaling for diffusion models beyond scaling denoising steps, 2025. [6](#)
- [40] Navonil Majumder, Chia-Yu Hung, Deepanway Ghosal, Wei-Ning Hsu, Rada Mihalcea, and Soujanya Poria. Tango 2: Aligning diffusion-based text-to-audio generations through direct preference optimization. In *Proceedings of the 32nd ACM International Conference on Multimedia*, page 564–572. Association for Computing Machinery, 2024. [2](#)
- [41] Sarthak Mittal, Korbinian Abstreiter, Stefan Bauer, Bernhard Schölkopf, and Arash Mehrjou. Diffusion based representation learning. In *Proceedings of the 40th International Conference on Machine Learning*. JMLR.org, 2023. [6](#)
- [42] Long Ouyang, Jeffrey Wu, Xu Jiang, Diogo Almeida, Carroll Wainwright, Pamela Mishkin, Chong Zhang, Sandhini Agarwal, Katarina Slama, Alex Ray, John Schulman, Jacob Hilton, Fraser Kelton, Luke Miller, Maddie Simens, Amanda Askell, Peter Welinder, Paul F Christiano, Jan Leike, and Ryan Lowe. Training language models to follow instructions with human feedback. In *Advances in Neural Information Processing Systems*, pages 27730–27744. Curran Associates, Inc., 2022. [2](#)
- [43] Dustin Podell, Zion English, Kyle Lacey, Andreas Blattmann, Tim Dockhorn, Jonas Müller, Joe Penna, and Robin Rombach. Sdxl: Improving latent diffusion models for high-resolution image synthesis. *ArXiv*, abs/2307.01952, 2023. [2](#), [7](#), [14](#)
- [44] Alec Radford, Jong Wook Kim, Chris Hallacy, Aditya Ramesh, Gabriel Goh, Sandhini Agarwal, Girish Sastry, Amanda Askell, Pamela Mishkin, Jack Clark, Gretchen Krueger, and Ilya Sutskever. Learning transferable visual models from natural language supervision. In *Proceedings of the 38th International Conference on Machine Learning*, pages 8748–8763, 2021. [7](#), [14](#)
- [45] Rafael Rafailov, Archit Sharma, Eric Mitchell, Christopher D Manning, Stefano Ermon, and Chelsea Finn. Direct preference optimization: Your language model is secretly a reward model. *Advances in Neural Information Processing Systems*, 36:53728–53741, 2023. [3](#), [4](#)
- [46] Aditya Ramesh, Prafulla Dhariwal, Alex Nichol, Casey Chu, and Mark Chen. Hierarchical text-conditional image generation with clip latents. *ArXiv*, abs/2204.06125, 2022. [2](#)
- [47] Robin Rombach, Andreas Blattmann, Dominik Lorenz, Patrick Esser, and Björn Ommer. High-resolution image synthesis with latent diffusion models. pages 10674–10685, 2022. [7](#)
- [48] Chitwan Saharia, William Chan, Saurabh Saxena, Lala Li, Jay Whang, Emily L Denton, Kamyar Ghasemipour, Raphael Gontijo Lopes, Burcu Karagol Ayan, Tim Salimans, Jonathan Ho, David J Fleet, and Mohammad Norouzi. Photorealistic text-to-image diffusion models with deep language understanding. In *Advances in Neural Information Processing Systems*, pages 36479–36494, 2022. [2](#)
- [49] Christoph Schuhmann, Romain Beaumont, Richard Vencu, Cade Gordon, Ross Wightman, Mehdi Cherti, Theo Coombes, Aarush Katta, Clayton Mullis, Mitchell Wortsman, Patrick Schramowski, Srivatsa Kundurthy, Katherine Crowson, Ludwig Schmidt, Robert Kaczmarczyk, and Jenia Jitsev. Laion-5b: An open large-scale dataset for training next generation image-text models. In *Advances in Neural Information Processing Systems*, pages 25278–25294, 2022. [7](#), [14](#)

- [50] Noam Shazeer and Mitchell Stern. Adafactor: Adaptive learning rates with sublinear memory cost, 2018. 7
- [51] Guibao Shen, Luozhou Wang, Jiantao Lin, Wenhao Ge, Chaozhe Zhang, Xin Tao, Yuanhui Zhang, Pengfei Wan, Zhong ming Wang, Guangyong Chen, Yijun Li, and Yingcong Chen. Sg-adapter: Enhancing text-to-image generation with scene graph guidance. *ArXiv*, abs/2405.15321, 2024. 3, 7
- [52] Jiaming Song, Chenlin Meng, and Stefano Ermon. Denoising diffusion implicit models. In *International Conference on Learning Representations*, 2020. 2, 4, 14, 16, 18
- [53] Yoad Tewel, Omri Kaduri, Rinon Gal, Yoni Kasten, Lior Wolf, Gal Chechik, and Yuval Atzmon. Training-free consistent text-to-image generation. *ACM Trans. Graph.*, 43: 52:1–52:18, 2024. 2
- [54] Ye Tian, Ling Yang, Xincheng Zhang, Yunhai Tong, Mengdi Wang, and Bin Cui. Diffusion-sharpening: Fine-tuning diffusion models with denoising trajectory sharpening. *ArXiv*, abs/2502.12146, 2025. 6
- [55] Masatoshi Uehara, Yulai Zhao, Kevin Black, Ehsan Hajiramezani, Gabriele Sciala, Nathaniel Lee Diamant, Alex M Tseng, Sergey Levine, and Tommaso Biancalani. Feedback efficient online fine-tuning of diffusion models. In *Proceedings of the 41st International Conference on Machine Learning*, pages 4889–48918. PMLR, 2024. 2
- [56] Pascal Vincent. A connection between score matching and denoising autoencoders. *Neural Computation*, 23(7):1661–1674, 2011. 6
- [57] Bram Wallace, Meihua Dang, Rafael Rafailov, Linqi Zhou, Aaron Lou, Senthil Purushwalkam, Stefano Ermon, Caiming Xiong, Shafiq Joty, and Nikhil Naik. Diffusion model alignment using direct preference optimization. pages 8228–8238, 2024. 2, 3, 4, 6, 7, 14, 16
- [58] Ruichen Wang, Zekang Chen, Chen Chen, Jian Ma, Haonan Lu, and Xiaodong Lin. Compositional text-to-image synthesis with attention map control of diffusion models. pages 5544–5552, 2024. 3
- [59] Yunnan Wang, Ziqiang Li, Wenyao Zhang, Zequn Zhang, Baao Xie, Xihui Liu, Wenjun Zeng, and Xin Jin. Scene graph disentanglement and composition for generalizable complex image generation. In *The Thirty-eighth Annual Conference on Neural Information Processing Systems*, 2024. 3, 6
- [60] Zixiao Wang, Hongtao Xie, Yuxin Wang, Jianjun Xu, Boqiang Zhang, and Yongdong Zhang. Symmetrical linguistic feature distillation with clip for scene text recognition. In *Proceedings of the 31st ACM International Conference on Multimedia*, page 509–518. Association for Computing Machinery, 2023. 3
- [61] Yang Wu, Pengxu Wei, and Liang Lin. Scene graph to image synthesis via knowledge consensus. pages 2856–2865, 2023. 3
- [62] Jinheng Xie, Yuexiang Li, Yawen Huang, Haozhe Liu, Wentian Zhang, Yefeng Zheng, and Mike Zheng Shou. Boxdiff: Text-to-image synthesis with training-free box-constrained diffusion. pages 7452–7461, 2023. 3
- [63] Jiazhen Xu, Xiao Liu, Yuchen Wu, Yuxuan Tong, Qinkai Li, Ming Ding, Jie Tang, and Yuxiao Dong. Imagereward: learning and evaluating human preferences for text-to-image generation. In *Proceedings of the 37th International Conference on Neural Information Processing Systems*, 2024. 2
- [64] Yilun Xu, Shangyuan Tong, and T. Jaakkola. Stable target field for reduced variance score estimation in diffusion models. In *ArXiv*, 2023. 6
- [65] Kai Yang, Jian Tao, Jiafei Lyu, Chunjiang Ge, Jiaxin Chen, Weihao Shen, Xiaolong Zhu, and Xiu Li. Using human feedback to fine-tune diffusion models without any reward model. pages 8941–8951, 2024. 2, 6, 7
- [66] Ling Yang, Zhilin Huang, Yang Song, Shenda Hong, G. Li, Wentao Zhang, Bin Cui, Bernard Ghanem, and Ming-Hsuan Yang. Diffusion-based scene graph to image generation with masked contrastive pre-training. *ArXiv*, abs/2211.11138, 2022. 3, 7
- [67] Ling Yang, Zhaochen Yu, Chenlin Meng, Minkai Xu, Stefano Ermon, and Bin Cui. Mastering text-to-image diffusion: Recaptioning, planning, and generating with multimodal LLMs. In *Proceedings of the 41st International Conference on Machine Learning*, pages 56704–56721, 2024. 3
- [68] Shentao Yang, Tianqi Chen, and Mingyuan Zhou. A dense reward view on aligning text-to-image diffusion with preference. In *Proceedings of the 41st International Conference on Machine Learning*, pages 55998–56032. PMLR, 2024. 2
- [69] Po-Hung Yeh, Kuang-Huei Lee, and Jun cheng Chen. Training-free diffusion model alignment with sampling demons. In *The Thirteenth International Conference on Learning Representations*, 2025. 7
- [70] Xincheng Zhang, Ling Yang, Yaqi Cai, Zhaochen Yu, Kaini Wang, Jiakexie, Ye Tian, Minkai Xu, Yong Tang, Yujiu Yang, and Bin Cui. Realcompo: Balancing realism and compositionality improves text-to-image diffusion models. *ArXiv*, abs/2402.12908, 2024. 3
- [71] Xincheng Zhang, Ling Yang, Guohao Li, Yaqi Cai, Jiakexie, Yong Tang, Yujiu Yang, Mengdi Wang, and Bin Cui. Itercomp: Iterative composition-aware feedback learning from model gallery for text-to-image generation. *ArXiv*, abs/2410.07171, 2024. 2, 6, 7
- [72] Ziyi Zhang, Li Shen, Sen Zhang, Deheng Ye, Yong Luo, Miaojing Shi, Bo Du, and Dacheng Tao. Aligning few-step diffusion models with dense reward difference learning. *ArXiv*, abs/2411.11727, 2024. 2
- [73] Dewei Zhou, You Li, Fan Ma, Zongxin Yang, and Yi Yang. Migc++: Advanced multi-instance generation controller for image synthesis. *ArXiv*, abs/2407.02329, 2024. 3
- [74] Dewei Zhou, You Li, Fan Ma, Xiaoting Zhang, and Yi Yang. Migc: Multi-instance generation controller for text-to-image synthesis. pages 6818–6828, 2024. 3
- [75] Shengzhe Zhou, Zejian Li, Shengyuan Zhang, Lefan Hou, Changyuan Yang, Guang Yang, Zhiyuan Yang, and Lingyun Sun. Reducing spatial fitting error in distillation of denoising diffusion models. In *Proceedings of the Thirty-Eighth AAAI Conference on Artificial Intelligence and Thirty-Sixth Conference on Innovative Applications of Artificial Intelligence and Fourteenth Symposium on Educational Advances in Artificial Intelligence*. AAAI Press, 2024. 4

- [76] Yufan Zhou, Bingchen Liu, Yizhe Zhu, Xiao Yang, Changyou Chen, and Jinhui Xu. Shifted diffusion for text-to-image generation. pages 10157–10166, 2023. [2](#)

## Supplementary Material

### S7. User Study

To evaluate the alignment between the generated image and human cognition, we design a user study involving two control groups: the group of SDXL [43] vs. Inversion DPO and the group of Diffusion-DPO [57] vs. Inversion-DPO. For each control group, we randomly select 500 pairs of images. In each trial, users are presented with two images and their corresponding prompts (text descriptions), one pair coming from SDXL and Inversion-DPO, and the other from Diffusion-DPO and Inversion-DPO. Users’ task is to choose the image that best matched the corresponding prompt. It is important to note that some of the generated images contain inappropriate content, so we remove a few images to ensure the experiment adhered to ethical guidelines and to prevent any potential negative impact.

The study invite 10 participants, with a gender ratio of 1:1, and ages ranging from 20 to 30. Participants come from diverse backgrounds, including computer science, design, and human-computer interaction (HCI).

In the comparison between SDXL and Inversion-DPO, 66.53% of users select the image generated by Inversion-DPO, while only 33.47% chose the image generated by SDXL. In the comparison between Diffusion-DPO and Inversion-DPO, Inversion-DPO has a higher selection rate of 72.67%, while Diffusion-DPO has only 27.33%. Based on the results of these two control experiments, Inversion-DPO shows a clear user preference, whether compared with SDXL or Diffusion-DPO. Particularly in the comparison with Diffusion-DPO, the selection rate for Inversion-DPO was significantly higher, indicating that Inversion-DPO has a distinct advantage in terms of content alignment and consistency with human cognition when generating images.

**Human Subjects Notification.** Before the experiment began, we provided a notification to the participants to inform them about the collection and use of data.

Dear volunteers, thank you for your support of our research. We are studying an image generation algorithm that can generate high-quality images based on user-provided text prompts. All information about your participation in this study will be included in the study records. All information will be processed and stored according to the local privacy laws and policies. Your name will not appear in the final report. When referring to your data, only the individual number assigned to you will be mentioned.

The use of user data has been approved by the Institutional Review Board of the primary author’s affiliation.

### S8. Additional Generation Examples

Inversion-DPO demonstrates a highly competent capability in image generation, achieving visually impressive and

high-quality results, as illustrated in Fig. S6. However, it is necessary to acknowledge that the model is not immune to failure cases. Typical failure modes include structural inconsistencies such as distorted legs, wings, or heads, as well as incorrect finger counts, as shown in the examples in Fig. S10.

### S9. Additional Explanation of Efficiency

In addition to the relationship between training steps and PickScore [26] presented in the main paper, we also report the correlations between training steps and Aesthetics Score [49] (Fig. S7), as well as between training steps and CLIP Score [44] (Fig. S8). Under identical training configurations, Inversion-DPO consistently outperforms Diffusion-DPO across all metrics, while also demonstrating faster convergence. Notably, even under constrained training conditions due to hardware limitations, Inversion-DPO still surpasses the officially released Diffusion-DPO in final performance.

### S10. Visual Interpretation of the Underlying Assumptions

In our derivation, a key assumption based on DDIM inversion [52] is that the values of  $x_{t-1}^w$  are similar when obtained from the inversion of  $x_0^w$  and from the forward sampling of  $x_T^w$ . To assess the validity of this assumption, we perform real-time visualization of the distributions along both the inversion and sampling trajectories. As illustrated in Fig. S9, the visual representations at corresponding time steps exhibit high similarity in both the forward and reverse processes, providing intuitive evidence that supports the reliability of this assumption.

### S11. Detailed Derivation of InversionDPO

We present detailed derivation of the final loss of InversionDPO. We begin with the form as

$$\log \frac{p_\theta(x_{0:T}^w)}{p_{\theta_0}(x_{0:T}^w)} = \sum_{t=1}^T [\log p_\theta(x_{t-1}^w | x_t^w) - \log p_{\theta_0}(x_{t-1}^w | x_t^w)] \quad (\text{S18})$$

Given the  $x_{1:T}^w$  by DDIM Inversion, we derive the following computation within the expectation. Specifically,  $\log \frac{p_\theta(x_{0:T}^w)}{p_{\theta_0}(x_{0:T}^w)}$  is first decomposed into the differences in conditional probabilities at each time step:

$$\log \frac{p_\theta(x_{0:T}^w)}{p_{\theta_0}(x_{0:T}^w)} = \sum_{t=1}^T [\log p_\theta(x_{t-1}^w | x_t^w) - \log p_{\theta_0}(x_{t-1}^w | x_t^w)] \quad (\text{S19})$$

Since  $p_\theta$  and  $p_{\theta_0}$  share the same distribution of  $x_T$  as standard Gaussian,  $\log p_\theta(x_T^w) - \log p_{\theta_0}(x_T^w)$  cancel out. The

User Preference	Other Methods	Inversion-DPO
SDXL vs Inversion-DPO	0.3347	0.6653
Diffusion-DPO vs Inversion-DPO	0.2733	0.7267

Table S4. Comparison of user preference between different image generation methods. In the comparison, Inversion-DPO consistently shows a higher preference from users, indicating its better alignment with human cognition and image content.



Figure S6. More high-quality and visually appealing generation examples.

conditional probabilities of  $p_\theta$  and  $p_{\theta_0}$  are Gaussian distributions as in equation 8 and becomes dirac-delta as  $\sigma_t$  approaches 0.

Given the assumption of inversion in Sec. 3.2, the values of  $\mathbf{x}_{t-1}^w$  are similar in the inversion from  $\mathbf{x}_0^w$  and in the sampling from  $\mathbf{x}_T^w$ . Therefore,  $\log p_\theta(\mathbf{x}_{t-1}^w|\mathbf{x}_t^w)$  is only related to  $\sigma_t^2$  and thus constant. At the same time, we have for  $p_{\theta_0}$  its expectation is

$$\boldsymbol{\mu}_{\theta_0}(\mathbf{x}_t^w) = \frac{\sqrt{\alpha_{t-1}}}{\sqrt{\alpha_t}} \mathbf{x}_t^w + \quad (\text{S20})$$

$$\left( \sqrt{1 - \alpha_{t-1} - \sigma_t^2} - \frac{\sqrt{\alpha_{t-1}(1 - \alpha_t)}}{\sqrt{\alpha_t}} \right) \epsilon_{\theta_0}(\mathbf{x}_t^w, t) \quad (\text{S21})$$

Therefore, we have

$$-\log p_{\theta_0}(\mathbf{x}_{t-1}^w|\mathbf{x}_t^w) = \frac{\|\boldsymbol{\mu}_{\theta_0}(\mathbf{x}_t^w) - \mathbf{x}_{t-1}^w\|^2}{2\sigma_t^2} + C \quad (\text{S22})$$

Since  $\mathbf{x}_{t-1}^w$  is equivalently generated by  $p_\theta$  (i.e.,  $\mu_\theta$ ) based on the assumption above, we further assume  $\mathbf{x}_{t-1}^w$

subjects to  $\mathcal{N}(\mu_\theta(\mathbf{x}_t^w), \sigma_t^2 I)$ . By substituting it, we have the simplified form  $\frac{1}{2\sigma_t^2} \|\boldsymbol{\mu}_\theta - \boldsymbol{\mu}_{\theta_0}\|^2$ . Transforming the mean difference into the difference in epsilon prediction, and denoting the mean as  $\boldsymbol{\mu}_\theta = \frac{1}{\sqrt{\alpha_t}} \mathbf{x}_t^w - \frac{\sqrt{1-\alpha_t}}{\sqrt{\alpha_t}} \epsilon_\theta(\mathbf{x}_t^w, t)$ , we obtain:

$$\|\boldsymbol{\mu}_\theta - \boldsymbol{\mu}_{\theta_0}\|^2 = \frac{1 - \alpha_t}{\alpha_t} \|\epsilon_\theta(\mathbf{x}_t^w, t) - \epsilon_{\theta_0}(\mathbf{x}_t^w, t)\|^2 \quad (\text{S23})$$

Summing the contributions across all time steps, we can arrive at:

$$\log \frac{p_\theta(\mathbf{x}_{0:T}^w)}{p_{\theta_0}(\mathbf{x}_{0:T}^w)} = \sum_{t=1}^T \frac{1 - \alpha_t}{2\sigma_t^2 \alpha_t} \|\epsilon_\theta(\mathbf{x}_t^w, t) - \epsilon_{\theta_0}(\mathbf{x}_t^w, t)\|^2, \quad (\text{S24})$$

We adopt the simple form as in DDPM [17] to eliminate the weights and coefficients. Therefore, taking the winning and

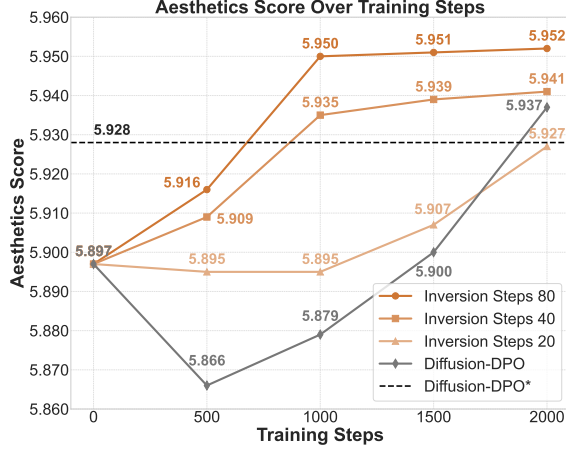


Figure S7. Relationship between training steps and Aesthetics Score improvements. The orange curve shows the performance of our Inversion-DPO trained with different numbers of DDIM inversion steps. The gray curve represents our implementation of Diffusion-DPO [57], while the dashed line corresponds to the officially released weights of Diffusion-DPO. All models are trained under identical configurations.

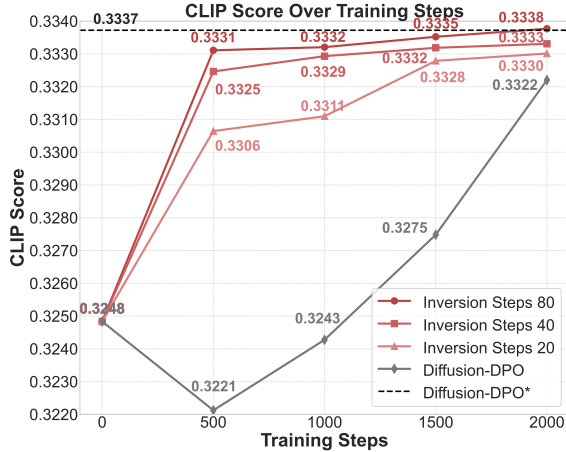


Figure S8. Relationship between training steps and CLIP Score improvements. The red curve shows the performance of our Inversion-DPO trained with different numbers of DDIM inversion steps. The gray curve represents our implementation of Diffusion-DPO [57], while the dashed line corresponds to the officially released weights of Diffusion-DPO. All models are trained under identical configurations.

lossing sample all together, we reach the final loss as

$$\mathcal{L}_{\text{Inversion-DPO}}(\theta) = -\mathbb{E}_{(\mathbf{x}_0^w, \mathbf{x}_0^l)} \log \sigma \left( \beta \mathbb{E}_{\substack{\mathbf{x}_{1:T}^w \sim p_\theta(\mathbf{x}_{1:T}^w | \mathbf{x}_0^w) \\ \mathbf{x}_{1:T}^l \sim p_\theta(\mathbf{x}_{1:T}^l | \mathbf{x}_0^l)}} \left[ \left\| \epsilon_\theta(\mathbf{x}_t^w, t) - \epsilon_{\theta_0}(\mathbf{x}_t^w, t) \right\|^2 - \left\| \epsilon_\theta(\mathbf{x}_t^l, t) - \epsilon_{\theta_0}(\mathbf{x}_t^l, t) \right\|^2 \right] \right) \quad (\text{S25})$$

Model	PickScore <sup>↑</sup>	CLIP <sup>↑</sup>	Aesthetic <sup>↑</sup>
Diffusion-DPO ( $q$ )	0.227	0.340	6.05
Inversion-DPO ( $p_\theta$ )	0.228	0.341	6.11
Diffusion-DPO <sup>†</sup> ( $q$ )	0.212	0.324	5.73
Inversion-DPO <sup>†</sup> ( $p_\theta$ )	0.212	0.325	5.73

Table S5. Performance impact of approximating the reverse distribution  $p_\theta$  with the forward  $q$ . In Inversion-DPO, the true reverse distribution  $p_\theta$  is utilized, whereas Diffusion-DPO relies on its approximation  $q$ .

## S12. Impact of the imprecise approximation

In Diffusion-DPO, due to the inaccessibility of the reverse trajectory, the posterior sampling  $p_\theta(x_{1:T}|x_0)$  is approximated by the noisy process  $q(x_{1:T}|x_0)$ . We argue that this approximation introduces non-negligible training errors and conduct an ablation study to investigate this effect. While Inversion-DPO involves recovering the whole noise trajectory across multiple time steps for alignment, in the code implementation, the original Diffusion-DPO samples a single timestep from  $q(x_{1:T}|x_0)$  and augment with a value  $T$  to obtain the final result. Such difference may also introduce performance discrepancy. For a fair comparison, we also evaluate Inversion-DPO by randomly sampling a single timestep from  $p_\theta(x_{1:T}|x_0)$ . As presented in Tab. S5 in SDXL and SD1.5, training with DDIM Inversion with  $p_\theta$  consistently yields better results than approximation based on the forward distribution  $q$ , highlighting the necessity and effectiveness of the core insight behind Inversion-DPO.

## S13. A Brief Introduction of Stable Diffusion

Diffusion models, such as Denoising Diffusion Probabilistic Models (DDPMs) [17] and Denoising Diffusion Implicit Models (DDIMs) [52], provide a generative modeling framework that is based on the gradual corruption of data through a noise injection process followed by the recovery of the original data. These models leverage a Markov chain process to progressively add Gaussian noise to the data in a forward process, and then learn to reverse this process to recover the data from noisy samples.

In DDPM, the forward process is a Markov chain where data  $x_0$  is progressively perturbed by Gaussian noise at each timestep, with the perturbation increasing over time. The transition between timesteps  $x_{t-1}$  and  $x_t$  is governed by a Gaussian distribution:

$$q(x_t|x_{t-1}) = \mathcal{N}(x_t; \sqrt{1 - \beta_t}x_{t-1}, \beta_t I),$$

where  $\beta_t$  is the noise variance at timestep  $t$ , and the forward process gradually transforms the data  $x_0$  into pure noise  $x_T$ . The reverse process, which is modeled during

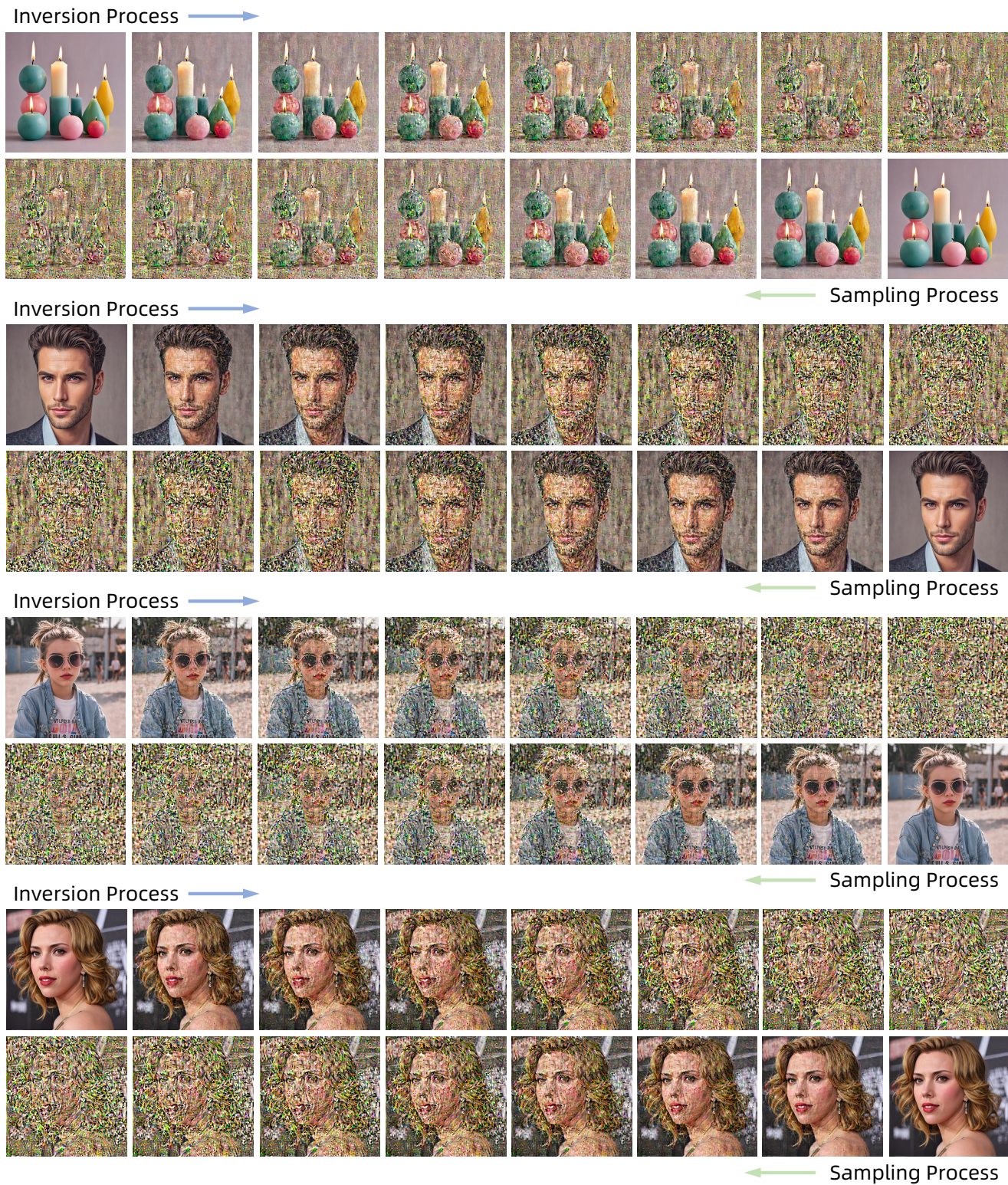


Figure S9. Visualization of data distributions in the inversion and sampling processes.

training, aims to recover the data by learning to reverse the noisy transformations:

$$p_{\theta}(x_{t-1}|x_t) = \mathcal{N}(x_{t-1}; \mu_{\theta}(x_t, t), \Sigma_{\theta}(x_t, t)).$$

The model is trained by optimizing the evidence lower bound (ELBO), which involves minimizing the difference between the forward and reverse process distributions. This training objective can be written as:

$$\mathcal{L}_{\text{simple}} = \mathbb{E}_{x_0, \epsilon, t} \left[ \left\| \epsilon - \epsilon_{\theta}(\sqrt{\bar{\alpha}_t}x_0 + \sqrt{1 - \bar{\alpha}_t}\epsilon, t) \right\|^2 \right],$$

where  $\epsilon_{\theta}$  is the model’s prediction of the noise added at each timestep, and  $\epsilon$  is Gaussian noise. This loss function allows the model to learn to predict the noise at each timestep, effectively learning the reverse process.

To accelerate the sampling process, [52] introduces DDIMs, which extend DDPMs by generalizing the forward process to be non-Markovian. This modification allows for a more efficient sampling process that reduces the number of steps required to generate high-quality samples. In DDIMs, the generative process is deterministic, and the model can sample from fewer timesteps while maintaining high sample quality. The key insight behind DDIMs is that the reverse process in DDPM can be reparameterized using a deterministic trajectory, which simplifies the sampling process significantly.

## S14. Limitation

Despite the effectiveness of our proposed Inversion-DPO framework, several limitations remain. First, the DDIM Inversion process relies on a strong assumption that the noise distribution in the forward (diffusion) and reverse (denoising) processes is consistent. Such assumption is valid only when the number of inversion steps is large enough. In practice, with a small inversion step, this assumption may potentially introduce inaccuracies in the reconstructed trajectories. Second, the training pipeline requires two rounds of inference: one from the pretrained model  $p_{\theta_0}$  to obtain the DDIM-inverted noise trajectories, and another from the reference model  $p_{\theta}$  to estimate the output distribution. This two inferences improve the convergence but increase training time and computational cost. Finally, the exact impact of the errors introduced by DDIM inversion remains unclear, and their influence on the overall optimization process warrants further investigation. More accurate Inversion methods may lead to more precision approximation. We present some failure cases in Fig. S10. Such failure may be a result of insufficient training or inadequate training data for alignment.

## S15. Social Impact

Our work enhances preference optimization in diffusion models, offering improved controllability and sample qual-

ity. However, this also introduces potential risks. Automated preference signals, if not carefully designed, may inadvertently promote unsafe or biased content due to metric misalignment. Moreover, there exists the possibility of malicious misuse, where adversarial inputs could manipulate the optimization to favor harmful or misleading generations. We advocate for incorporating rigorous safety filters, human oversight, and transparent evaluation practices to mitigate such risks and ensure responsible deployment.



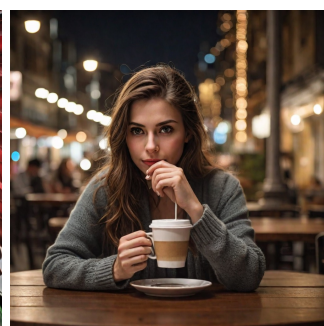
An image of a beautiful cute young European woman standing in karate stance ready to fight in a full contact karate match wearing a sports bra, kumite gloves, karate pants and karate blackbelt, barefoot.

(a)



Red and green eagle.

(b)



An woman sitting on a table drinking coffee, long shot, wide shot, highly detailed, intricate, professional photography, RAW color perfect photo, night shot, bokeh, sharp focus, taken with eos 5d, UHD 8k.

(c)



An image hyper realistic of a dog in the sky with dragon wings.

(d)

Figure S10. Additional results of failure examples.